Determination of the Attenuation for Ice Ih – Magnesium Chloride Hydrate Eutectics and Their Effects on the Thermomechanical Evolution of Europa.

Thomas B. Czernik, Cameron Meyers, Greg Hirth, Reid F. Cooper, Brown University, Department of Earth, Environmental, and Planetary Sciences, Providence, Rhode Island 02912.

Introduction: We present results from experiments performed to determine the attenuation of Ice Ih – magnesium chloride hydrate eutectics at planetary conditions relevant to Europa. On Europa, the periodic tidal flexing (at frequency $f = 3 \times 10^{-6}$ Hz) contributes the dominant stress on the shell of the satellite [1,2]. Due to anelastic (± plastic) tidal flexing, strain energy in the shell is converted into heat. For this case, the heating rate ($\dot{E}$) is proportional to the attenuation of a mechanical input, Q^{-1}, along with several other well-determined physical and orbital factors [3]. Q^{-1} is the largest unknown variable regarding the quantification of the energy budget of the satellite; our goal is to use an experimental approach to constrain the attenuation of the shell on Europa.

Europa's subsurface ocean is a brine, and the salt(s) have expression in the solid shell; given the temperatures involved, a secondary, crystalline salt-hydrate phase (or phases) is expected. Spectroscopy data suggest that magnesium chloride hydrate, specifically $MgCl_2 \cdot 12H_2O$, is a dominant secondary phase [4-6].

Method: Specimens were crystallized from homogenous brine solutions using two selected bulk compositions - a eutectic composition of H_2O-$MgCl_2 \cdot 12H_2O$ (20.6 wt% $MgCl_2$, 79.4 wt% H_2O) and a hypoeutectic composition (7.7 wt% $MgCl_2$, 92.3 wt% H_2O). Both the rate at which the brine is cooled and, particularly, the degree of undercooling (ΔT below the eutectic temperature, ΔT^{Eu} — Fig. 1) affect microstructure [7-9], specifically the scale of ice–hydrate phase intercalation. Solidification was performed at two undercoolings below the eutectic temperature ($\Delta T_{Eu} \approx -5$ °C and –15 °C; Fig. 1). Undercooling temperature was maintained using an isothermal bath in which an ethanol plus-ethylene glycol liquid solution was mixed with dry ice; the three-phase, three chemical component bath fixes the temperature (within ±1.5°C) based on the composition of the solution [10]. Prior to deformation, microstructural analysis was performed using micrographs obtained from a Zeiss Sigma VP field emission scanning electron microscope (FE-SEM) with a Gatan Aalto 2500 cryogenic attachment.

Uniaxial compressive cyclic loading experiments were performed using a servomechanical-actuator apparatus retrofitted with a cryogenic chamber ($-60 \leq T_{chamber}$ (°C) ≤ -48). Displacements of loaded specimens were measured *in situ* with a linear variable differential transformer (LVDT). Ice-hydrate specimens were subjected to a servo-controlled median stress (σ_m = 0.25-1 MPa) superimposed with a sinusoidally varying cyclic stress (amplitude σ_0 = 0.01–0.21 MPa, oscillatory frequency f = 0.0005 - 0.01 Hz). Initially, specimens were held at the median stress before cyclic loading was superimposed until a constant creep rate was observed. An iterative least squares estimation with a convergence tolerance of 10^{-8} on both the residual sum of squares and the fit coefficients was used to generate nonlinear fits to the mechanical data. The strain due to steady state creep at the median stress was subsequently removed from the fits to isolate the strain due to the oscillatory stress. Q^{-1} was then determined from the tangent of the angle of which stress lags strain (δ) for the creep-corrected stress-strain curves (i.e., $Q^{-1} = \tan\delta$). Uncertainty on Q^{-1} measurements reflects the standard deviation normalized by the amount of experiments performed (3) for one specimen under the same set conditions. Q^{-1} values were calculated using between 3-30 consecutive cycles. The number of cycles included for analysis of any experiment was chosen based on the residuals of the fit.

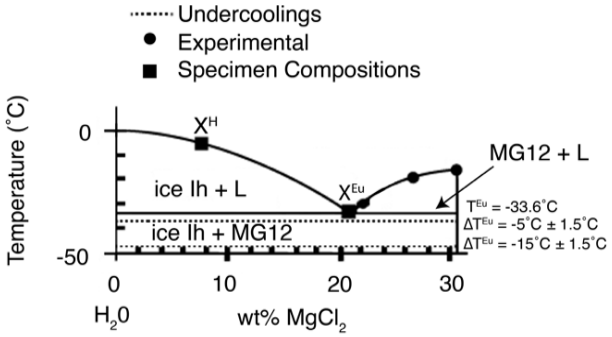

Figure 1 An ambient-pressure phase diagram of the $MgCl_2 \cdot 12H_2O$ - H_2O system adapted from Dubois and Marignac (1997) [11]. Experimental points were used for liquidus curve fitting. Compositions of prepared specimens (X^{Eu} =20.6 wt% $MgCl_2$, X^H = 7.7 wt% $MgCl_2$) and the two undercoolings are marked.

Eutectic Microstructure: FE-SEM micrographs of specimens of both selected bulk compositions and both undercoolings demonstrate typical eutectic structures, which include a high spatial density of crystalline heterophase boundaries created by cooperative solidification (Fig. 2). Phase maps were generated from the micrographs by producing binary images using ImageJ software; images were first converted to an 8-bit grayscale and subsequently a threshold value was chosen as the dividing point between the two phases, based on visual inspection. Contrast was adjusted to enhance areas of relief and thus clearly distinguish between phases, such that phases could be mapped. Phase area fractions were calculated using ImageJ and matched predicted volume fractions within ±2%. In addition to FE-SEM, specimen elemental compositions were measured locally by energy dispersive X-ray spectroscopy (EDS).

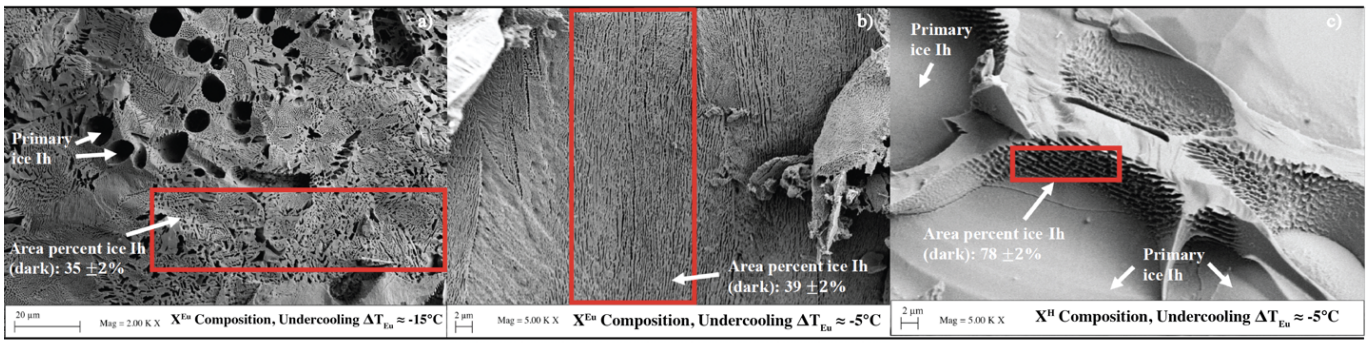

Figure 2 Micrographs of solid ice-hydrate specimens with different compositions and undercoolings. Phase fractions were analyzed within the marked red box. Error on reported phase fractions reflect variations imposed by adjusting the contrast. Ice Ih preferentially sublimates, thus dark areas of relief are interpreted to be ice Ih and light areas the hydrate.

Results: We report initial results of Q^{-1} for the eutectic-composition specimens solidified at modest undercoolings ($\Delta T_{Eu} \approx -5$ °C) as a function of frequency for $T_{chamber}$ = -54 ± 6 °C, varying median stress, and varying oscillatory stress (Fig. 3). In general, the Q^{-1} data set displays a modest power-law dependence ($Q^{-1} \propto f^{-\varphi}$, $\varphi \approx 0.2$) and with exclusion of outliers, falls within a single order of magnitude. The data acquired at lower frequencies ($f \leq 0.003$Hz) are more clustered than data acquired at higher frequencies, suggesting a transition of different physical mechanisms determining the attenuation response within different regimes.

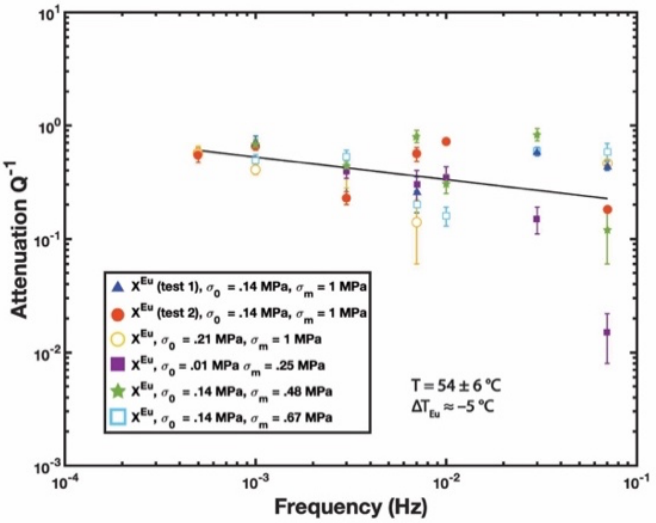

Figure 3 Q^{-1} vs frequency for eutectic composition specimens. Undercooling, temperature during the experiment ($T_{chamber}$) and a modest power law trend are marked (black line). Uncertainties on the experimental temperature reflect the maximum range of fluctuation over the length of an experiment.

Discussion/Planetary Implications: Our current results suggest that the attenuation of ice-hydrate solids is comparable to that of polycrystalline ice determined from previous experiments at similar conditions [12]. This result is unexpected because metallurgical studies indicate that eutectic materials tend to combine the antithetical properties of high stiffness and high attenuation [13-14]. If the unique properties shown in metallurgical studies were to hold, and if the surface of Europa is composed of eutectic material, then the icy shell is anticipated to simultaneously be more dissipative, stiffer and stronger (perhaps more brittle?) than one composed of pure ice—with ramifications for understanding both shell thickness and convection behavior. However in the context of our results, further microstructural analyses will need to be made to assess scaling of the data to planetary conditions.

Acknowledgements: The SEM data was acquired at the RI Consortium for Nanoscience and Nanotechnology, a URI College of Engineering core facility partially funded by the National Science Foundation EPSCoR, Cooperative Agreement #OIA-1655221.

References: [1] Barr A. C. and A. P. Showman (2009) *Europa*, *405-430*. [2] Tobie G. et al. (2003) *JGR*, *108.* [3] Peale S. J. and Cassen P. (1978) *Icarus, 36(2), 245-269*. [4] Brown M.E. and Hand K.P. (2013) *AJ*, *145.* [5] Ligier N. et al. (2016) *AJ*, 51 [6] Vu T. H. et al. (2016) *AJL*, *816.* [7] Porter D. A. et al. (2009) *Phase Trans. in Met. and Alloys (3rd Ed.)*. [8] Hunt J.D. and Jackson K.A. (1966) *AIME Transactions, 236*. [9] Croker M.N. et al (1973) *R. Soc.*, *335*. [10] Lee D.W. and Jensen C.M. (2000) *JCE, 77.* [11] Dubois M. and Marignac C. (1997) *Econ. Geol.*, *92*. [12] McCarthy C. and Cooper R. F. (2016) *EPSL*, *443*. [13] Brodt M. and Lakes R.S. (1996) *J. Mater. Sci., 31*. [14] Buechner P. et al. (1999) *Scr. Mater., 41*.